Communications

Inaccuracies in Numerical Calculation of Scattering near Natural Frequencies of Penetrable Objects

G. L. Hower, R. G. Olsen, J. D. Earls, and J. B. Schneider

Abstract—**Calculated scattering from a nonconducting cylindrical ring shows great variability to small changes in the material or geometric parameters within certain ranges of these parameters. The observations are explained by a resonance phenomenon in which the operating frequency is found to lie close to a complex natural frequency of the scattering object. Note that this resonance is a real, observable effect predicted by analytical solutions and not the "spurious" numerical resonances which have been widely discussed and which one wishes to suppress. Attempts have been made to reproduce near resonance scattering results using the method of moments and finite-difference time-domain codes. These have failed despite the use of widely accepted discretization densities. Thus, the existence of such resonances requires additional care when interpreting computed results for scattering from similar nonconducting objects having electric and/or magnetic properties.**

I. Introduction

Recent efforts intended to test a method of moments (MOM) computer code for scattering from two-dimensional objects have involved computation of scattering from a nonconducting ring. This object is a convenient choice (used, for example, by Richmond [1]) since analytical results are available for comparison. The appropriate expressions are obtained by a straightforward solution of the boundary value problem and consist of infinite series of Bessel functions.

For the case of an incident plane wave, the bistatic scattering patterns obtained with the computer code showed an unexpected sensitivity to small changes in the material parameters of the ring, permittivity (ϵ) and permeability (μ), within certain ranges of the parameter values. In addition, the patterns obtained by the computer code using cell sizes with dimensions of about $0.1\lambda_d$ (where λ_d is the wavelength in the material) compared favorably with values obtained using the series solution except within these same regions. For these particular ranges of parameter values, a much finer level of discretization was required to obtain results comparable to those from the series solution. The latter results were obtained at the expense of greatly increased computation times.

In this communication, we present a sample of the observations mentioned above and an explanation in terms of a "resonance" effect. Resonance effects for dielectric cylinders of high permittivity have been suggested earlier by Van Bladel [2], [3]. The results of the present study have implications whenever it is necessary to interpret numerical computations of scattering from objects similar to the case considered here, i.e., nonconductors having electric and/or magnetic properties.

II. Discrepancies Between MOM and Exact Solution

A method of moments code was developed to study scattering from conducting and penetrable objects with general cylindrical cross sections. The problem was formulated in terms of equivalent electric and magnetic volume polarization currents radiating in free space

Manuscript received May 1, 1992; revised February 1, 1993.

The authors are with the School of Electrical Engineering and Computer Science, Washington State University, Pullman, WA 99164-2752.

IEEE Log Number 9211265.

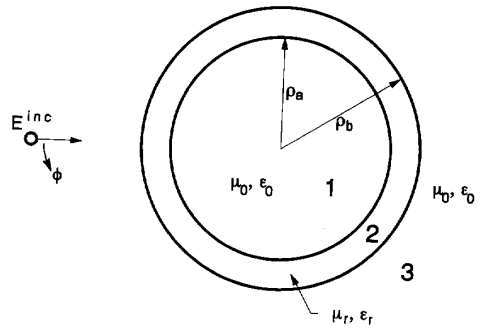

Fig. 1. Geometry of the nonconducting ring.

[4], [5]. The cross section of the object was discretized by dividing it into rectangular cells, using pulse functions to expand the unknown polarization currents and point matching at the cell centroids to obtain linear equations for the unknowns. Since, in general, both electric and magnetic properties are assumed, the resulting equation is a combination of the electric (EFIE) and magnetic (MFIE) field integral equations. Self terms involving integrals of the Hankel function, $H_0^{(2)}(k_0 R)$, required special treatment. The singularity was extracted by subtracting and adding the small argument approximation to the Hankel function. This yields two terms. The first has a well-behaved integrand and may be integrated numerically. The second (logarithmic) term may be integrated analytically over the rectangular surface of the self-element. Further details of the numerical method are given in an earlier report [6].

One problem studied in the process of validating the code was the hollow nonconducting ring shown in Fig. 1. An incident wave polarized along the axis of the cylinder is assumed (TM). By duality, the results also apply directly to a TE incident wave if the values of ϵ and μ are interchanged. The outer and inner diameters of the ring were $0.6\lambda_0$ and $0.5\lambda_0$ respectively where λ_0 is the free-space wavelength. The relative permeability (μ_r) of the object was assumed to be 4.0 while the relative dielectric constant (ϵ_r) was allowed to take on several values.

Results for the bistatic radar cross section (RCS) generated by the MOM code for two different dielectric constants are plotted in Fig. 2. For this figure, the average size of the rectangular cells used was approximately $0.09\lambda_d$ by $0.09\lambda_d$ (where λ_d is the wavelength in the medium). This level of discretization (i.e., approximately 100 unknowns per square dielectric wavelength) is recommended by Peterson and Klock based on calculations of the interior fields of dielectrics [7]. The total number of cells (i.e., unknowns) used was 324. Also shown in each plot is the bistatic RCS generated by the "exact" series solution. Clearly there is good agreement between the exact and numerical solutions for $\epsilon_r = 9.5$ but relatively poor agreement for $\epsilon_r = 10.0$. The remainder of this paper is an attempt to understand the reasons for such discrepancies.

III. Attempts to Reconcile Differences

The first attempt to reconcile the differences was to recompute the numerical solution with smaller rectangular discretizations. The

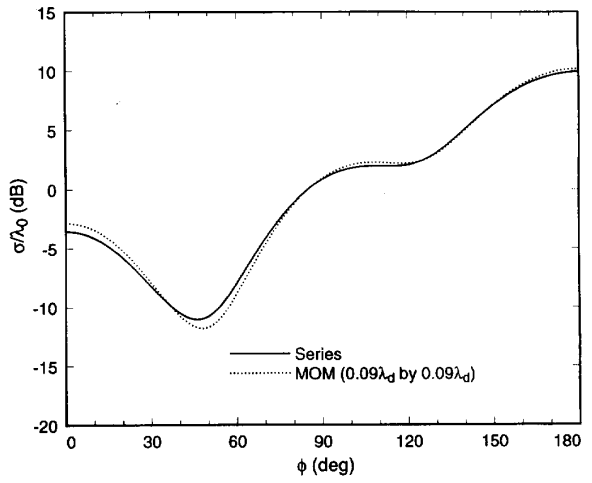

(a)

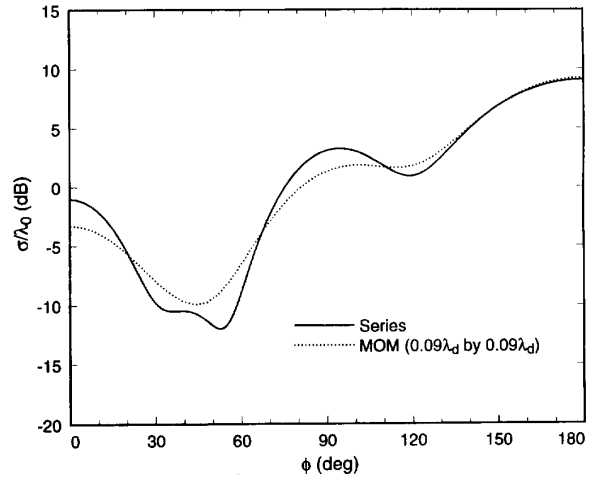

(b)

Fig. 2. Bistatic RCS plots (MOM): $\rho_a = 0.25\lambda_0$, $\rho_b = 0.30\lambda_0$, $\mu_r = 4.0$. (a) $\epsilon_r = 9.5$; (b) $\epsilon_r = 10.0$.

results of such a study do indeed show an improvement in the computed curves as the level of discretization is increased. However, good results can only be obtained at the expense of a considerable increase in computer time. Thus, this does not appear to be an acceptable way to solve the problem.

A second option is to borrow the "equal area" or "equal volume" concept which has been used for studying scattering from perfect conductors and by Peterson and Klock for dielectric/dielectric interfaces [7], [8]. In two-dimensional problems with a surface integral formulation, this would require that the perimeter of the discretized interfaces be forced to be equal to the actual perimeters while for a volume integral formulation, the discretized cross section of the scattering object should have the same area as the actual object. These criteria require adjusting the radii (ρ_a and/or ρ_b) for the MOM calculations. At the level of discretization used in the present study, such adjustments did not produce any discernible improvements in the results.

It is also possible that the lack of agreement between the moment method results and the series solution is an artifact of the moment

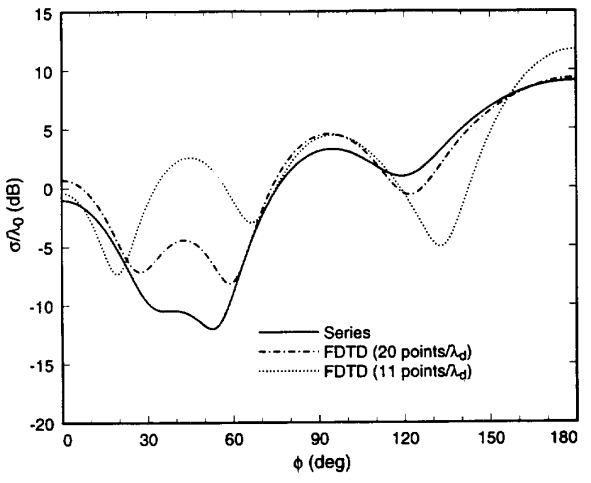

Fig. 3. Bistatic RCS plots (FDTD): $\rho_a = 0.25\lambda_0$, $\rho_b = 0.30\lambda_0$, $\mu_r = 4.0$, $\epsilon_r = 10.0$.

method code used. To test this hypothesis we used the finite-difference time-domain (FDTD) method [9], [10] to independently calculate the bistatic RCS of the dielectric cylinders. FDTD is a direct solution of Maxwell's equations that employs central difference approximations over a finite grid. Far-field quantities can be easily obtained [11]. The FDTD code used to generate the results in this section employed the second-order Mur absorbing boundary condition, and the bistatic RCS was calculated in a manner similar to the one found in [11]. The code used a uniform grid spacing and we approximated the cylindrical scatterer by a "staircase" structure.

The scatterer was centered in a square grid that had sides approximately twice as long as the free-space wavelength (λ_0). Fig. 3 presents a comparison of the analytic series solution with results obtained from the FDTD method when $\epsilon_r = 10.0$ and $\mu_r = 4.0$. The FDTD calculations were performed using grid spacings of 11 and 20 points per wavelength in the dielectric (λ_d). An improvement is evident for the finer grid spacing and these numerical results behave in a manner similar to those obtained from the moment method. For $\epsilon_r = 9.5$ and $\mu = 4.0$ the series solution and FDTD results show good agreement (comparable to the agreement seen in Fig. 2(a)).

IV. Series Solution

The analytical solution for scattering from a dielectric ring proceeds in much the same way as common solutions for scattering from a perfectly conducting cylinder [12], [13]. The fields in each region of Fig. 1 are expanded as an infinite series of appropriate Bessel functions, and the necessary conditions on the tangential fields at the boundaries are enforced to give a matrix equation of the following form:

$$[A_n][C_n] = [S_n]. \tag{1}$$

In this expression $[C_n]$ is a column vector of the unknown coefficients, $[S_n]$ is a column vector of known terms, and $[A_n]$ is a square matrix of known terms. After solving this system of equations, the scattered field in region three may be expressed as

$$E_z^{\text{scat}} = E_0 \sqrt{\frac{2}{\pi\beta_0\rho}} e^{-j(\beta\rho - \pi/4)} \cdot [a_0 + ja_1 \cos\phi - a_2 \cos 2\phi - ja_3 \cos 3\phi + a_4 \cos 4\phi + \cdots]. \tag{2}$$

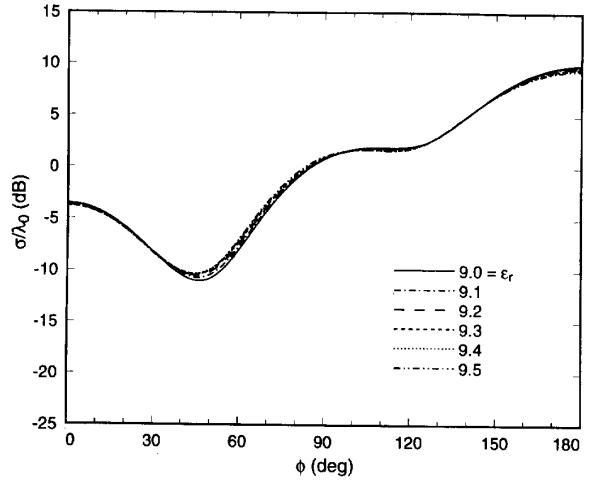

(a)

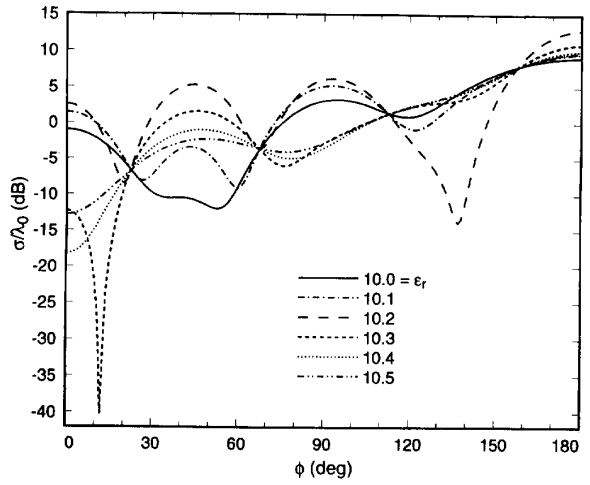

(b)

Fig. 4. Bistatic RCS plots (series solution): $\rho_a = 0.25\lambda_0, \rho_b = 0.30\lambda_0$, $\mu_r = 4.0$. (a) $9.0 \leq \epsilon_r \leq 9.5$; (b) $10.0 \leq \epsilon_r \leq 10.5$.

where ρ and ϕ are the usual cylindrical coordinates and the RCS would be proportional to $|E_z^{\text{scat}}|^2$.

This analytical solution has been used to obtain the RCS plots of Fig. 4. Fig. 4(a) for $9.0 \leq \epsilon_r \leq 9.5$ displays the expected behavior with only small changes in the RCS for small changes in permittivity. Fig. 4(b), however, exhibits much larger variations in RCS for similarly small changes in ϵ_r. For example, the 2% change of permittivity from 10.0 to 10.2 produces a more than 20 dB variation in RCS. Additional curves were plotted for $1.0 \leq \epsilon_r \leq 11.0$. Within this range of ϵ_r, regions of high variability were observed in the vicinity of $\epsilon_r = 7.2$ and 10.2 (the latter is shown in Fig. 4(b)). The variations are found to be stronger when ϵ_r is near 10.2 and the range of ϵ_r values over which significant variability occurs is narrower for ϵ_r near the 10.2 than for ϵ_r near 7.2.

For values of ϵ_r near 10.2 and 7.2, the same variability in scattering patterns is observed for small changes in μ_r or in the dimensions, ρ_a or ρ_b. For example, a change in ρ_a from $0.25\lambda_0$ to $0.2495\lambda_0$ produces a significant change in the scattering pattern for the case $\epsilon_r = 10.2$ and $\mu_r = 4.0$.

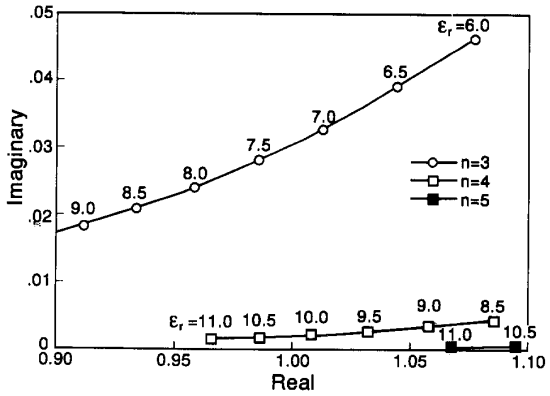

Fig. 5. Location of zeros in normalized complex frequency plane.

The extreme sensitivity to parameters which is evident in Fig. 4(b) suggests a resonance phenomenon. Natural modes of the scattering object would occur at frequencies for which the determinant of matrix $[A_n]$ is zero:

$$|A_n| = F(\omega) = 0. \tag{3}$$

Although in the present case there are no real values of ω that satisfy this equation because of radiation losses, we note that if $|A_n|$ is small for a particular n, the corresponding a_n in (2) will become large. Thus, a particular $\cos n\phi$ term will dominate. Physically, this implies a "quasi-resonance" condition of the nonconducting ring inside which a portion of the energy of the incident wave is nearly "trapped" even though total reflection at the boundaries does not occur. We should note that the resonance condition referred to here is in the exact solution and hence is observable. This is in contrast to the resonance condition that has been studied in the context of scattering by perfect conductors [14]. In the latter case, the resonance condition is an artifact of the mathematical method used to solve the problem and should be suppressed.

To investigate the resonance possibility in the present problem, we made use of a zero-search code [15], to see if complex zeros for (3) exist, for any value of n, near the real frequency used in the previous calculations (normalized to unity). For the set of parameters, $\mu_r = 4.0$, $6 \leq \epsilon_r \leq 11$, zeros were found in the complex plane near the normalized driving frequency for the $n = 3$, 4, and 5 terms. The trajectories of these zeros are shown in Fig. 5. Not only do complex zeros exist in the vicinity of the operating frequency, the closest approach indeed does occur near the expected values of $\epsilon_r \simeq 10.2$ and 7.2. Note that in the former case, the approach is much closer, which would imply a sharper, narrower resonance than for the latter case, as was also observed.

An observation that further verifies the validity of the interpretation presented here is the presence of "nodes" in the scattering patterns of Fig. 4(b), where computed values of RCS remain constant with respect to changes in ϵ_r. For the case of ϵ_r values near 10.2, the complex zero that occurs near $\omega = 1$ is in the $n = 4$ term of the series. This implies a dominance of the $\cos 4\phi$ term in the scattered field expression. Since $\cos 4\phi$ is zero at $\phi = 22.5°$, $67.5°$, $112.5°$, and $157.5°$, we would expect "nodes" in its RCS pattern at these angles exactly as observed in Fig. 4(b). For $\epsilon_r \approx 7.2$, the complex zero is in the $n = 3$ term so that the $\cos 3\phi$ variation would dominate and the nodal points would be expected at $\phi = 30°$, $90°$, and $150°$, which was verified by further computations.

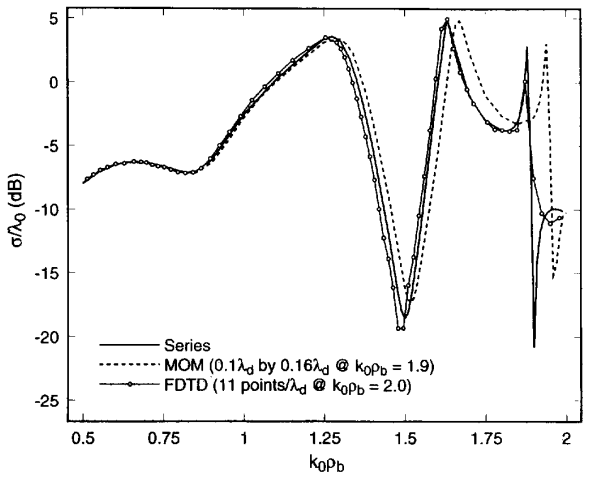

(a)

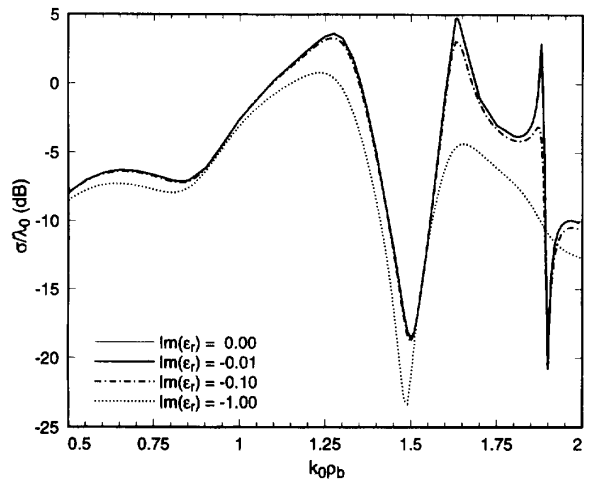

(b)

Fig. 6. Backscatter RCS versus frequency ($k_0\rho_b$) for a fixed ring: $\rho_a = 0.25$ m, $\rho_b = 0.30$ m, $\mu_r = 4.0$. (a) $\epsilon_r = 10.2$; (b) $\epsilon_r = 10.2 + jI_m(\epsilon_r)$.

V. Frequency Shift of Numerical Results

We have found that it is possible to obtain agreement between series and numerical solutions (with $\approx 0.1\lambda_d$ cell size) if geometric or electrical parameters are slightly altered. Given this, it would be interesting to know if the numerical results plotted as a function of frequency are simply a frequency shifted version of the series solution. To study this question, results from MOM, FDTD, and series methods have been plotted in Fig. 6, which shows the backscatter RCS versus $k_0\rho_b$—e.g., backscatter from a particular cylindrical ring ($\rho_a = 0.25m$, $\rho_b = 0.30m$, $\epsilon_r = 10.2$, $\mu_r = 4.0$) as the frequency is varied. The MOM results in this case were obtained for a fixed number of cells (240) corresponding to a worst case cell size of about $0.1\lambda_d \times 0.16\lambda_d$ near the right-hand side of the curve. One observation that can be made is the extremely narrow resonance that occurs near $k_0\rho_b = 1.9$. This behavior is expected given the results shown in Figs. 4(b) and 5. It is also useful to note that similar narrow resonances have been observed, for example, in the context of scattering from dielectric coated spheres [16]. Another observation is that the MOM result is essentially a frequency shifted version of the exact result. Further, because the resonances are so narrow, differences of up to 20 dB in the results may be observed.

The FDTD calculations used 11 points/λ_d and a computational domain of approximately $3\lambda_0 \times 3\lambda_0$ at the highest frequency. Third-order Liao absorbing boundary conditions were used [17], [18]. Like the MOM results, the FDTD results agree well with the series solution at the lower frequencies. Additionally, as the frequency is increased, these results appear to be a shifted form of the exact series results. However, the shift is in the opposite direction from MOM and the amount of shift does not appear to be proportional to the frequency. As the frequency continues to increase, the FDTD results fail to track the exact results acceptably. This is undoubtedly due in large part to the staircase approximation of the continuously varying scatterer surface—the scatterer geometry is too coarsely approximated to obtain accurate scattered fields in the vicinity of the strong resonance near $k_0\rho_b = 1.9$.

It is evident that the accuracy of numerical methods for scattering calculations depends on the proximity of the driving frequency to complex natural frequencies of the object. Since real materials are lossy, it is important to also study the effect of losses on these conclusions. It is well known that the natural frequencies plotted in Fig. 5 will generally be moved further from the real axis as the loss is increased. This results in a corresponding decrease in the influence of natural frequencies on scattering. The quantitative effect of loss can be observed in Fig. 6(b). Here, the loss of the hollow ring with the (otherwise) same parameters as Fig. 6(a) was increased and the scattering recomputed. Clearly if the imaginary part of the relative dielectric constant has a value less than -0.01, the results shown earlier are still valid. Since many common materials are less lossy than this at microwave frequencies [19], the inaccuracies described here should be observable. According to Fig. 6(b), however, larger values of loss can cause the resonance effect to be greatly reduced and result in a significant change in the scattering.

VI. Conclusions

The extreme variability in results observed in moment method and finite-difference time-domain computations of scattering from a nonconducting ring are well explained by the resonance phenomenon discussed above. The possibility of these resonances requires care in interpreting numerical results for scattering from similar objects. This is because the use of widely accepted discretization densities and/or the equal area criteria do not guarantee correct results. While the use of conformal elements may resolve the problem [20], [21], this has not yet been demonstrated for near resonant scattering. For practical cases where no *a priori* knowledge of a complex resonance frequency exists, computed results over a small range of one of the parameters should be examined. If considerable variation occurs, the results should be interpreted cautiously.

Acknowledgment

The authors wish to acknowledge the efforts of S. Unger and J. McPherson in developing the computer code for the MOM and series calculations.

References

[1] J. H. Richmond, "Scattering by a dielectric cylinder of arbitrary cross-section shape," *IEEE Trans. Antennas Propagat.*, vol. 13, pp. 334–341, May 1965.

[2] J. Van Bladel, "Scattering of low-frequency waves by dielectric cylinders," *IEEE Trans. Antennas Propagat.*, vol. 24, pp. 255–258, Mar. 1976.

[3] J. Van Bladel, "Radar echoes near a dielectric resonance," *Electron. Lett.*, vol. 17, no. 19, pp. 699–700, Sept. 1981.

[4] A. J. Poggio and E. K. Miller, "Integral equation solution of three-dimensional scattering problems," in *Computer Techniques for Electromagnetics*, R. Mittra, Ed. New York: Pergammon Press, 1973.
[5] E. L. Roetman, R. P. Kochhar, and G. L. Hower, "An integral representation for the fields in electromagnetic scattering problems," *Electromagnetics*, vol. 12, pp. 1–15, 1992.
[6] S. R. Unger, "Electromagnetic scattering from cpated perfectly conducting cylinders," Washington State University Rep. No. 3, BPO #B-245-389, Nov. 1989.
[7] A. F. Peterson and P. W. Klock, "An improved MFIE formulation for TE-wave scattering from lossy, inhomogeneous dielectric cylinders," *IEEE Trans. Antennas Propagat.*, vol. 36, pp. 45–49, Jan. 1988.
[8] J. J. H. Wang, *Generalized Moment Methods in Electromagnetics*. New York: John Wiley & Sons, 1991, pp. 192–193.
[9] K. S. Yee, "Numerical solution of initial boundary value problems involving Maxwell's equations in isotropic media," *IEEE Trans. Antennas Propagat.*, vol. 14, pp. 302–307, 1966.
[10] A. Taflove, "Review of the formulation and applications of the finite-difference time-domain method for numerical modeling of electromagnetic wave interactions with arbitrary structures," *Wave Motion*, Vol. 10, pp. 547–582, 1988.
[11] A. Taflove and K. Umashankar, "Radar cross section of the general three-dimensional scatterers," *IEEE Trans. Electromagn. Compat.*, vol. 25, pp. 433–440, 1983.
[12] R. F. Harrington, *Time-Harmonic Electromagnetic Fields*. New York: McGraw Hill, 1961.
[13] C. A. Balanis, *Advanced Engineering Electromagnetics*. New York: John Wiley & Sons, 1989.
[14] J. R. Mautz and R. F. Harrington, "A combined-source solution for radiation and scattering from a perfectly conducting body," *IEEE Trans. Antennas Propagat.*, vol. 27, pp. 445–454, July 1979.
[15] P. R. Brazier-Smith and J. F. M. Scott, "On the determination of the roots of dispersion equations by use of winding number integrals," *J. Sound and Vibration*, vol. 145, no. 3, pp. 503–510, 1991.
[16] J. Rheinstein, "Scattering of electromagnetic waves from dielectric coated conducting spheres," *IEEE Trans. Antennas Propagat.*, Vol. 12, pp. 334–340, May 1964.
[17] Z. Liao, H. L. Wong, B. Yang, and Y. Yuan, "A transmitting boundary for transient wave analyses," *Scientia Sinica A*, vol. 27, no. 10, pp. 1063–1076, 1984.
[18] W. C. Chew, *Waves and Fields in Inhomogenous Media*. New York: Van Nostrand Reinhold, 1990.
[19] D. M. Pozar, *Microwave Engineering*. Reading, MA: Addison-Wesley, 1990.
[20] R. D. Graglia, "The use of parametric elements in the moment method solution of static and dynamic volume integral equations," *IEEE Trans. Antennas Propagat.*, vol. 36, pp. 636–646, May 1988.
[21] T. G. Jurgens, A. Taflove, K. Umashankar, and T. G. Moore, "Finite-difference time-domain modeling of curved surfaces," *IEEE Trans. Antennas Propagat.*, vol. 40, no. 4, pp. 357–366, 1992.

Efficient Method for Analysis and Design of Aperture-Coupled Rectangular Microstrip Antennas

Mohammad A. Saed

***Abstract*—This paper describes a method for the analysis and design of rectangular microstrip antennas coupled through a small aperture to a microstrip feed line in a two-layer configuration. The technique is numerically efficient, making it suitable for computer-aided design. The analysis takes into account higher order modes excited underneath the patch. Analysis results were implemented in two computer programs: an analysis program and a design program based on optimization techniques. Experimental results are presented to validate this method.**

Manuscript received July 20, 1992; revised November 23, 1992.
The author is with the Department of Electrical Engineering, State University of New York, College at New Paltz, New Paltz, NY 12561.
IEEE Log Number 9211266.

I. Introduction

Microstrip patches can be fed using one of four techniques: a microstrip line directly connected to the patch [1]–[4], probe feeding [5]–[7], aperture or slot coupling [8]–[12], and electromagnetic coupling [13], [14]. Aperture- or slot-coupled patches have the advantage that they are amenable to multilayer structures where integration of the feed network and necessary electronic control components is feasible, without the need for drilling holes, as in probe-fed patches. This paper concerns the analysis and design of aperture-coupled patches, which have been analyzed mainly using full-wave analysis techniques. Most of these techniques use an integral equation formulation [9] or a mode matching approach [12] coupled with a numerical method such as the method of moments to allow computer implementation. Even though these techniques are rigorous, their main disadvantage is that they are complex, computationally extensive, and time consuming, and they are not amenable to computer-aided design. However, using these techniques is a must when the simplifying assumptions of other methods break down (such as when the frequency operation is extended to the millimeter-wave region).

The method presented in this paper is an efficient method for analyzing and designing aperture-coupled microstrip patches when the patch substrate is electrically thin and the aperture is electrically small. Its results can also serve as a starting point for full-wave analysis techniques when more accuracy is needed. First, expressions are derived to allow the computation of the input impedance seen by the microstrip feed line for given aperture dimensions, aperture location, and feed line extension beyond the aperture. This is presented in Section II. The inverse process, which is the evaluation of aperture dimensions, location, and length of feed line extension to yield a desired input impedance, is described in Section III. Experimental results are presented in Section IV. Finally, some conclusions and observations are given in Section V.

II. Calculation of Input Impedance

The structure under consideration is shown in Fig. 1. The analysis of this structure uses the theory of coupling through small apertures originally proposed by Bethe [15]. Coupling through small apertures can be accounted for by using an equivalent electric current dipole, $\vec{J}$, and a magnetic current dipole, $\vec{M}$, located at the center of the aperture. The aperture is then replaced by a perfect conductor, thus splitting the structure into two regions: the feed line region (region a) and the patch region (region b). The current dipoles are related to the fields in the feed line region as follows:

$$\vec{J} = j\omega\epsilon_e^a \alpha_e \vec{E}_{an}\, \delta(x - x_0)\delta(y - y_0)\delta(z) \tag{1}$$

$$\vec{M} = -j\omega\mu_0 \alpha_m \vec{H}_{at}\, \delta(x - x_0)\delta(y - y_0)\delta(z), \tag{2}$$

where $\vec{E}_{an}$ and $\vec{H}_{at}$ are the normal component of the electric field and the tangential component of the magnetic field to the aperture in region a (the feed line region), ϵ_e^a is the effective dielectric constant in region a, α_e is the electric polarizability of the aperture, α_m is the magnetic polarizability of the aperture, δ is the impulse function, and $(x_0, y_0, 0)$ are the coordinates of the center of the aperture. The electric and magnetic polarizabilities of a circular aperture of radius r are given by $\alpha_e = 2r^3/3$, $\alpha_m = 4r^3/3$, and those for a rectangular aperture of length l_a and width d are $\alpha_e = \alpha_m = \pi l_a d^2/16$. The